Songklanakarin J. Sci. Technol.
36 (3), 375-387, May - Jun. 2014

SONGKLANAKARIN JOURNAL OF SCIENCE AND TECHNOLOGY
http://www.sjst.psu.ac.th

Original Article

Comparison of H-mode plasma simulations using toroidal velocity models depending on plasma current density and ion temperature in presence of an ITB

Boonyarit Chatthong* and Thawatchai Onjun

School of Manufacturing Systems and Mechanical Engineering,
Sirindhorn International Institute of Technology, Thammasat University, Khlong Luang, Pathum Thani, 12121 Thailand.

Received 14 June 2013; Accepted 19 February 2014

Abstract

Two different approaches for predicting plasma toroidal velocity (v_ϕ) are developed and used in self-consistent simulations of *H*-mode plasmas with the presence of ITB using BALDUR integrated predictive modelling code. In the first approach, the toroidal velocity depends on the plasma current density; while in the second approach the toroidal velocity is directly proportional to the ion temperature. The profile of v_ϕ is used to calculate the ω_{ExB} flow shear which is a main mechanism for plasma transport suppression, leading to the ITB formation. In all simulations, the core transport model is a combination of NCLASS neoclassical transport and semi-empirical Mixed Bohm/gyro-Bohm model that includes the ITB effects. The boundary condition is set at top of the pedestal and is estimated using a pedestal model based on a combination of magnetic and flow shear stabilization pedestal width scaling and an infinite-n ballooning pressure gradient. Two toroidal velocity models are used to simulate the time evolution of plasma temperature and density profiles of 10 JET discharges. The root mean square error (RMSE) is used to compare simulation results of those 10 JET discharges with experimental data. It is found that RMSE of T_i, T_e, n_e are 28.1%, 31.8%, and 15.0% for the first toroidal velocity model and 25.5%, 30.2%, and 15.1% for the second toroidal velocity model, respectively. Furthermore, this suite of codes is used to predict the ITER performance under standard type I ELMy *H*-mode. It is found that the simulation yields formation of a narrow ITB near *r/a* = 0.7 in the simulation using the current density dependent model and a wide ITB from *r/a* = 0.5 to 0.8 in the simulation using the ion temperature dependent model. The average of central ion temperature, total fusion power output and alpha power are predicted to be 36 keV, 159 MW and 492 MW for the current density dependent model and 49 keV, 218 MW and 786 MW for the ion temperature dependent model, respectively.

Keywords: ITB, *H*-mode, toroidal velocity, BALDUR, JET, ITER

1. Introduction

Currently, Magnetic Confinement Fusion (MFC) based on tokamak concept is the most advanced experimental machine in term of nuclear fusion energy production and is in the process to extend for nuclear fusion reactor. Production of significant fusion reactions inside a tokamak requires high plasma temperature and density, as well as a sufficient energy confinement time. One of the milestones in fusion research was marked by the discovery of high confinement mode (*H*-mode), which results from the formation of an Edge Transport Barrier (ETB) (Wagner *et al.*, 1982). Since the high confinement mode (*H*-mode) plasmas in tokamaks generally provide high temperature and excellent energy confinement time, burning fusion experiment such as ITER is designed to operate in the *H*-mode regime. It is widely accepted that the performance of an *H*-mode discharge can be further improved with the formation of a transport barrier inside the plasma, called an Internal Transport Barrier (ITB) (Connor

* Corresponding author.
Email address: boonyarit.chatthong@gmail.com

et al., 2004). The presence of both ETB and ITB in the plasma causes major improvement in core temperature, pressure, confinement time, and hence, fusion power production.

Simulation is one of the tools that can be used to study and learn about the plasma behavior. Due to the reliability and the speed of today's computer, the simulation codes can be integrated and complicated enough for the results to be trustworthy. A number of studies have been done on both simulating the existing tokamaks and predicting the future machine, like ITER (Bateman *et al.*, 2003; Budny *et al.*, 2008; Chatthong *et al.*, 2010; Chatthong *et al.*, 2011; Halpern *et al.*, 2008; Onjun *et al.*, 2005; Pianroj *et al.*, 2012; Roach *et al.*, 2008). There are various integrated predictive modeling codes such as CRONOS (Artaud *et al.*, 2010), JETTO (Cenacchi *et al.*, 1988), ASTRA (Pereverzev *et al.*, 2002), and BALDUR (Singer *et al.*, 1988), aiming to self-consistently predict plasma performance. They are run with a variety of transport models like MMM95 (Hannum *et al.*, 2001), GLF23 (Kinsey *et al.*, 2002), and Mixed B/gB (Tala *et al.*, 2002). Those works yielded a different range of results because, partly, different assumptions were used, such as initial conditions of heating power and plasma density, impurity condition, or even different transport models. In addition, many simulations are carried out to study ITER plasma. In Onjun *et al.* (2009), ITER with combined effects of both ITB and ETB was simulated to predict the performance of ITB *H*-mode plasma. Also the behaviors of impurity in ITER were studied and analyzed (Pianroj *et al.*, 2010) and the impact of pellet injection on ITB in ITER *H*-mode plasma (Leekhaphan *et al.*, 2011) and on ITER plasma without ITB (Klaywitthaphat *et al.*, 2012; Wisitsorasak *et al.*, 2011) were studied via simulation method as well. Recently, the effect of symmetry breaking via the application of non-axisymmetric field leading to an offset NTV toroidal rotation has been investigated in ITB ITER-like plasma using BALDUR code (Chatthong *et al.*, 2013).

There are several mechanisms involved in the formation of ITB. It is widely accepted that an ω_{ExB} flow shear plays a significant role in this phenomenon. According to (Burrell 1997), ω_{ExB} induces de-correlation of turbulent convective cells resulting in less transport of plasma heat and particles from its core. Thus, in the region with strong flow shear the transport is reduced to neoclassical level and the barrier is formed which is shown as plasmas having relatively high gradient temperature or density. Even though another mechanism like zonal flow (Diamond *et al.*, 2005) can also intrinsically generate the electric field shear, its role is omitted in this work. In the future work, it is interesting to incorporate the contribution of shear effects both from the zonal flow and the flow shear. It is found that the reduction of transport is associated with shear effects, especially the velocity shear and magnetic shear (Burrell, 1997). Theoretically, the calculation of ω_{ExB} is derived from the force balanced equation which requires information such as ion density, pressure gradient, poloidal velocity (v_θ) and toroidal velocity (v_ϕ). There have been studies of momentum and velocity transport in poloidal direction (Eriksson *et al.*, 2007, Rogister *et al.*, 2002; Rozhansky *et al.*, 2002; Tala *et al.*, 2007) but not much has been done on toroidal direction. There have been some theoretical works on toroidal velocity prediction like those in Callen *et al.* (2009), and Stacey (2004), but for simplicity, simple models are used in this work. An empirical model based on local ion temperature for predicting toroidal rotation was proposed (Chatthong *et al.*, 2010), it was then used to simulate ITER performance (Chatthong *et al.*, 2011). There is a doubt in the empirical model mainly because it was developed solely based on JET experimental data so its general validity especially its projection to the bigger machine like ITER is uncertain. In this paper, a new current density dependent toroidal velocity calculation is proposed and derived based on electromagnetism theory of charge flow, which could potentially remove the projection validity problem.

In this work, plasma spatiotemporal profiles including plasma current, ion and electron temperatures and densities are simulated self-consistently using BALDUR integrated predictive modeling code. The impact of ETB on plasma is expressed in terms of a pedestal model (Onjun *et al.*, 2002). This region is a raising pedestal at the edge of plasma and the gradient is assumed to be constant. The pedestal temperature is explained using the theory based pedestal width model combined with pressure gradient limits by ballooning mode instability. The pedestal width model is based on magnetic and flow shear stabilization ($\Delta \propto \rho_i s^2$) (Sugihara *et al.*, 2000). The model is found to be in agreement with experimental data within around 30% RMSE (Onjun *et al.*, 2002). The model for ITB used in this paper is based on literature review of ITB (both theoretical work and experimental work). It is called semi-empirical Mixed Bohm/gyroBohm (Mixed B/gB) core transport model which proposes that formation of ITB is caused by the suppression in anomalous transport due to ω_{ExB} flow shear and magnetic shear (Tala *et al.*, 2001). This model is successfully found to be in agreement with data from various JET experiments (Parail *et al.*, 1999; Parail, 2002; Tala *et al.*, 2005; Tala *et al.*, 2006; Tala *et al.*, 2001; Tala *et al.*, 2002). In BALDUR, data for ω_{ExB} is given to the code. Moreover, ω_{ExB} can be calculated from toroidal velocity through the force balance equation. In order to predict the future machine like ITER, it is important to develop a model estimating toroidal velocity. In addition, to be fully self-consistent, it is essential for BALDUR to be able to calculate, hence, ω_{ExB} from fundamental physics quantities such as geometrical data of each tokamak, density, current, magnetic field, temperature, etc. This paper focuses on the development of a current density dependentmodel for use in simulations of JET and prediction of ITER with combination of ITB and ETB. Theprofiles are also compared with those predicted by the ion temperature dependent model.

The paper is organized as follows: an introduction to simulation methods including the models used is discussed in section 2; the toroidal velocity models are presented in section 3; results of simulations and discussion are described in section 4; and a summary is given in section 5.

2. Simulation Methods

2.1 BALDUR

BALDUR integrated predictive modeling code (Singer *et al.*, 1988) is a time-dependent transport modeling code which is used to compute many physical quantities in tokamaks. The code itself simultaneously solves three diffusion equations of number density, energy density and poloidal magnetic field. It can be used to compute the profiles of plasma densities and temperatures as well as q profile. BALDUR code self-consistently computes plasma profiles by combining many physical processes together in the form of modular structures, for example, heat and particle transport, plasma heating, particle flux, boundary conditions, and sawtooth oscillations. It was found that results from BALDUR are in decent agreements with experimental data. For example, BALDUR simulations yielded an agreement of about 10% relative root mean square deviation (RMSD) for temperature and density profiles of H-mode JET and DIII-D plasmas (Hannum *et al.*, 2001).

2.2 Mixed B/gB model

Mixed B/gB is a semi-empirical anomalous transport model. It consists of a combination of Bohm and gyro-Bohm scaling. The Bohm model was first derived for electron transport for the JET tokamak (Taroni *et al.*, 1994). Then, it was modified to additionally describe ion transport (Erba *et al.*, 1995) with a Gyro-Bohm term. Usually, the Bohm term dominates over most of the plasma. The gyro-Bohm term contributes mainly in the deep core of the plasma and in small tokamaks with low heating power and low magnetic field. The Mixed B/gB model includes ITB effect by having a cut-off in Bohm term which is a step function of flow shear and magnetic shear. The model can be expressed as of the following (Tala *et al.*, 2002)

$$\chi_{\mathrm{e}} = 1.0\chi_{\mathrm{gB}} + 2.0\chi_{\mathrm{B}}, \tag{1}$$

$$\chi_{\mathrm{i}} = 0.5\chi_{\mathrm{gB}} + 4.0\chi_{\mathrm{B}}, \tag{2}$$

$$D_{\mathrm{H}} = D_{\mathrm{Z}} = \left(0.3 + 0.7\rho\right)\frac{\chi_{\mathrm{e}}\chi_{\mathrm{i}}}{\chi_{\mathrm{e}} + \chi_{\mathrm{i}}}, \tag{3}$$

with

$$\chi_{\mathrm{gB}} = 5\times10^{-6}\sqrt{\mathrm{T_e}}\left|\frac{\nabla \mathrm{T_e}}{B_\phi^2}\right|, \tag{4}$$

$$\chi_{\mathrm{B}} = \chi_{\mathrm{B_0}} \times \Theta\left(-0.14 + \mathrm{s} - \frac{1.47\omega_{\mathrm{E\times B}}}{\gamma_{\mathrm{ITG}}}\right), \tag{5}$$

$$\chi_{\mathrm{B_0}} = 4\mathrm{x}10^{-5} R\left|\frac{\nabla\left(n_e T_e\right)}{n_e B_\phi}\right| q^2\left(\frac{\mathrm{T_e}\left(0.8\rho_{\max}\right) - T_e\left(\rho_{\max}\right)}{\mathrm{T_e}\left(\rho_{\max}\right)}\right), \tag{6}$$

where χ_e (m^2/s) is the electron diffusivity, χ_i (m^2/s) is the ion diffusivity, χ_{gB} (m^2/s) is the gyro-Bohm contribution, χ_B (m^2/s) is the Bohm contribution, D_H (m^2/s) is the particle diffusivity, D_Z (m^2/s) is the impurity diffusivity, ρ is normalized minor radius, $\mathrm{T_e}$ (keV) is the local electron temperature, B_ϕ (T) is the toroidal magnetic field, s is the magnetic shear, ω_{ExB} (s^{-1}) is the shearing rate, γ_{ITG} (s^{-1}) is the linear growth rate, R (m) is the major radius, and n_e (m^{-3}) is the local electron density. The linear growth rate γ_{ITG} is calculated from v_{th}/qR, where v_{th} (m/s) is the electron thermal velocity.

The ω_{ExB} shearing rate can be calculated according to Hahm-Burrell model (Zhu *et al.*, 2000),

$$\omega_{ExB} = \frac{\left(RB_\theta\right)^2}{B_\phi}\frac{\partial\left(E_r / RB_\theta\right)}{\partial\psi}, \tag{7}$$

where B_θ is the poloidal magnetic field, Ψ is the poloidal flux, and E_r is the radial electric field, which can be calculated from the force balance equation as follows:

$$E_r = \frac{1}{Zen_i}\frac{\partial p_i}{\partial r} - v_\theta B_\phi + v_\phi B_\theta \tag{8}$$

where $\frac{\partial p_i}{\partial r}$ is the pressure gradient, n_{i} is the ion density, Z is the ion charge number, e is the elementary charge, and v_θ and v_ϕ are the poloidal and toroidal velocities, respectively. Note that the poloidal velocity is estimated using NCLASS (Houlberg *et al.*, 1997).

2.3 Pedestal model

For BALDUR calculation, the boundary conditions are set at the top of the pedestal, which is where the edge transport barrier (ETB) is observed. The pedestal region is located at the steep gradient right near the edge of the plasma. It is assumed that the pressure gradient ($\partial p / \partial r$) within this region is constant so the pedestal temperature (T_{ped}) can be calculated as follows (Onjun *et al.*, 2002):

$$T_{ped} = \frac{1}{2kn_{ped}}\Delta\left|\frac{\partial p}{\partial r}\right| \tag{9}$$

where n_{ped}(m^{-3}) is pedestal density, k is the Boltzmann's constant, and Δ is the pedestal width. So in order to calculate pedestal temperature one must obtain pedestal density, pedestal width and pedestal gradient. The pedestal density, n_{ped}, is obtained by an empirical model which is based on the fact that n_{ped} is a fraction of line average density, n_l, that can be taken from experimental data, as shown:

$$n_{ped} = 0.71 n_l \,. \tag{10}$$

This empirical pedestal density model agrees with the data from the International Tokamak Physics Activity (ITPA) pedestal database with 12% RMSE (Bateman *et al.*, 2003).

The pedestal pressure gradient scaling is limited by the ballooning mode instability (Connor 1998). It is based on the assumption that there exists a maximum normalized pressure gradient with critical pressure gradient, α_c

$$\alpha_c(s,\delta,\kappa) = -\frac{2\mu_0 R q^2}{B_\phi^{\,2}}\left(\frac{\partial p}{\partial r}\right)_c . \tag{11}$$

Here, δ is triangularity, κ is elongation, μ_0 is permeability of free space, R is the tokamak major radius, q is safety factor, and B_ϕ is vacuum toroidal magnetic field. The triangularity and elongation are the plasma parameters that define its cross section shape; detailed definition of these variables can be seen in Wesson *et al.* (2004). Note that this critical pressure gradient may implicitly depend on the magnetic shear, the triangularity and the elongation because these parameters can affect the safety factor and pressure gradient in the pedestal region. Rewriting this relation and substituting pressure gradient into equation (10) gives

$$T_{ped} = \frac{\Delta}{2kn_{ped}} \frac{\alpha_c B_\phi^{\,2}}{2\mu_0 R q^2} \tag{12}$$

The pedestal width scaling model is based on magnetic and flow shear stabilization ($\Delta \propto \rho_i s^2$) (Sugihara *et al.*, 2000). There is an assumption that the transport barrier is formed in the region where the turbulence growth rate is balanced by a stabilizing $E_r xB$ shearing rate. The scaling width is derived to be

$$\Delta = C_1 \rho s^2 = C_1\left(4.57x10^{-3}\frac{\sqrt{A_H T_{ped}}}{B_T}\right)s^2, \tag{13}$$

where C_1 is the constant of proportionality and A_H is the average hydrogenic mass. After combining this scaling with the previous pressure gradient scaling, the scaling of T_{ped} is as follows

$$T_{ped} = C_1^{\,2}\left(\left(\frac{4.57x10^{-3}}{4\mu_0\left(1.6022x10^{-16}\right)}\right)^2\left(\frac{B_\phi^{\,2}}{q^4}\right)\left(\frac{A_H}{R^2}\right)\left(\frac{\alpha_c}{n_{ped}}\right)^2 s^4\right). \tag{14}$$

This result is used in BALDUR code to calculate the pedestal temperature, which is the boundary condition of the transport model, and to eventually compute plasma profiles. The constant C_1 was chosen to minimize the RMSD with 533 experimental data points from four large tokamaks obtained from ITPA pedestal database. The constant was found to be 2.42 (Onjun *et al.*, 2002).

3. Models for Predicting Toroidal Velocity

3.1 Current density dependent approach

This model is based on the current density flow of charge, in which, for simplicity, it is assumed to be in term of drift velocity of plasma flow.

$$v_\phi = \frac{J_\phi}{en_{i,e} Z_{eff}}, \tag{15}$$

where J_ϕ represents the current density flow in toroidal direction which can be calculated in BALDUR via Ampere's law, $n_{i,e}$ is ion and electron density, and Z_{eff} is effective charge. Figure 1 shows normalized minor radius (*r/a*) comparison profile of experimental v_ϕ of JET discharge 40847 with current density in toroidal direction from the diagnostic simulation (simulation using toroidal velocity from experiment to construct the current profile) at the diagnostic time. It can be seen that the profiles are similar in which the values are high near the centre and low near the edge with relatively flat profiles at the regions close to both boundaries.

3.2 Ion temperature dependent approach

This model describes that the toroidal velocity is linearly proportional to the local ion temperature (T_i), the exact form is as follows:

$$v_\phi[m/s] = 1.43\times10^4 T_i\left[keV\right]. \tag{16}$$

It was developed and used to simulate JET data (Chatthong *et al.*, 2010). Then later it was used to predict ITER performance (Chatthong *et al.*, 2011), which illustrated that during plasma quasi-steady state the anomalous transport was suppressed over a wide region. The problem is that this model is empirically built based solely from data from JET tokamak. So the projection problem is rather

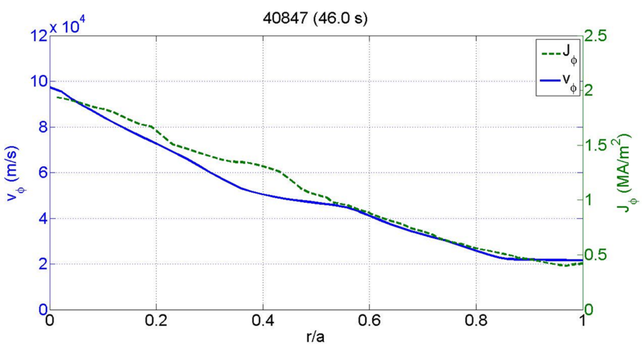

Figure 1. Profile plot of toroidal velocity v_ϕ (solid) together with toroidal current density J_ϕ (dashed) as a function of *r/a* for JET 40847 discharge at the diagnostic time.

Table 1. Summary of plasma parameters for 10 JET optimized shear discharges during their diagnostic time.

JET	Time (s)	R (m)	a (m)	I_p (MA)	B_ϕ (T)	κ	δ	$n_l (10^{19}\ m^{-3})$
40542	47	2.93	0.94	3.22	3.49	1.64	0.35	2.41
40847	46	2.92	0.96	2.85	3.50	1.56	0.20	2.33
46123	46.5	2.89	0.98	2.50	2.54	1.52	0.17	2.24
46664	45.7	2.92	0.94	2.95	3.50	1.71	0.20	2.27
51599	46	2.89	0.96	2.21	2.64	1.66	0.23	1.90
51976	46.3	2.92	0.95	2.40	3.49	1.69	0.26	2.45
52009	21.6	3.01	0.88	2.49	2.70	1.72	0.47	7.30
53521	49	2.89	0.97	2.00	3.54	1.63	0.21	2.99
53532	46.5	2.89	0.96	2.22	2.64	1.67	0.23	2.52
53537	46.5	2.90	0.96	2.22	2.64	1.67	0.23	2.15

questionable. Moreover, the set of experimental data used in the model development is mainly NBI (neutral beam injection)-heated plasma. In other words, the plasma is rotated toroidally by the external torque caused by NBI heating. This raises an important issue because ITER will be much larger (840 m^3 plasma volume compared to 100 m^3 of JET) so that the torque from NBI should not be enough to rotate it toroidally.

4. Results and Discussion

4.1 JET simulations

In this work, 10 JET optimized shear *H*-mode discharges with ITB formation (40542, 40847, 46123, 46664, 51599, 51976, 52009, 53521, 53532, and 53537) are chosen from the International Profile Database (Boucher *et al.*, 2000). Table 1 shows the summary of parameters from all 10 discharges used for the simulations where R is major radius, a is minor radius, I_p is plasma current, B_ϕ is toroidal magnetic field, κ is plasma elongation, δ is plasma triangularity and n_l is line average density.

4.1.1 Comparison

In this part, the predicted toroidal velocityfrom two models are compared. Examples ofprofile are shown in Figure 2. Each demonstratesas a function of r/a, the closed circles represent experimental data, the solid line with triangle markers represents simulation result of ion temperature dependent model, and the solid line represents simulation result of current density dependent model. Note that diagnostic time for each discharge is selected based on ITB and *H*-mode considerations. From this figure, it can be observed that the simulation results tend to over-predict the experiments. This is almost always the case for all 10 JET discharges. Furthermore, the general profile shape of the current density dependent model is rather unsmooth near the edge of the plasma where thevalues abruptly spike up and then decrease to zero right at the edge. This strange behaviour is a result of numerical procedure according to how BALDUR computes the current density. BALDUR assumes that the current is zero at the edge, the value at the next grid is high to conserve overall current flow.

Quantitatively, the root mean square error (RMSE) values between simulation results and experimental data are computed for comparison according to:

$$\mathrm{RMSE}(\%) = \sqrt{\frac{\sum_{i=1}^{N}\left(\ln\left(v_{\phi\_\exp_i}\right) - \ln\left(v_{\phi\_\mathrm{mod}_i}\right)\right)^2}{N-1}} \times 100, \tag{17}$$

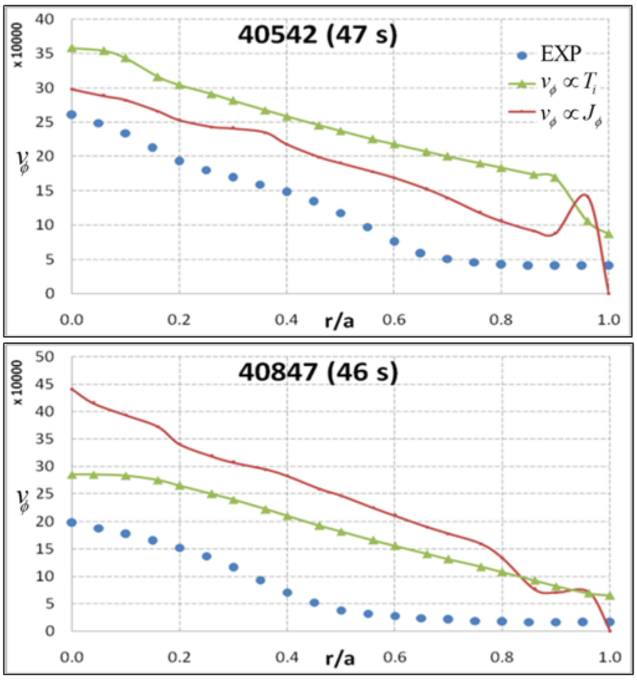

Figure 2. Comparison of toroidal velocity v_ϕ between experimental values (dots) and simulation results using ion temperature T_i dependent (solid-triangle) and current density J_ϕ dependent (solid) models for JET discharges 40542 (top) and 40847 (bottom) during their diagnostic time.

where $v_{\phi\_\exp}$ is the experimental value, v_{ϕ_mod} is the value calculated from the models, and N is total number of data points. The summary results are shown in Figure 3. The RMSE ranges from 16.99% to 200.5% for the current density dependent model, whereas it ranges from 18.58% to 55.50% for the ion temperature dependent model. The best agreement is found in the current density dependent prediction of discharge 51976, while the worst agreement is ironically found in the prediction using the same model of discharge 46664. The average RMSE of all 10 discharges is found to be 73.02% with the standard deviation of 60.81% for the current density dependent model, and found to be 37.09% with the standard deviation of 13.04% for the ion temperature dependent model. The average values imply that the prediction by ion temperature dependent model is better. However, if one observes discharge by discharge and also from the high standard deviation, one can see that it is possible that this current density dependent model can only capture a limited regime of the plasma. So for the applicable discharges, it can predict the profile rather adequately. While in some other discharges additional physics or models are needed.

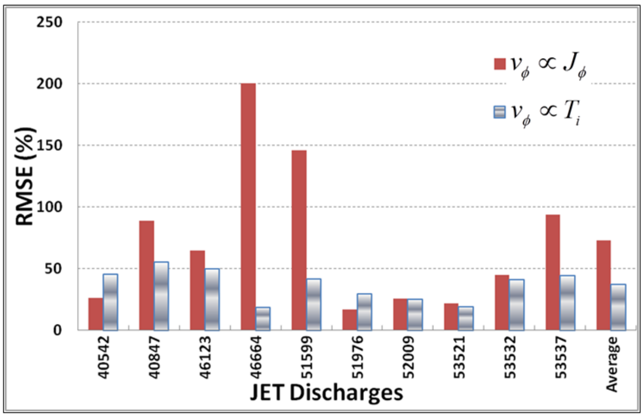

Figure 3. RMSE deviations of 10 JET discharges and their average for toroidal velocity v_ϕ using current density J_ϕ dependent (solid bars) and ion temperature T_i dependent (striped bars) models.

4.1.2 Simulation profiles

For simulations of each JET discharge, the time-evolution profiles of ion temperature (T_i), electron temperature (T_e), and electron density (n_e) are calculated and predicted by BALDUR. Figure 4 illustrates example profiles of JET discharges 40847 and 52009; note that the dots represent experimental data, the dashed line represents simulation results using current density dependent model, and the solid line represents simulation results using ion temperature dependent model. First of all, the figure shows that the simulation results over-predict both the temperatures and the density at the edge while they tend to under-predict the values at plasma center. In other words, the pedestal model yields higher predicted values and the Mixed B/gB model yields lower predicted values than the experimental data. Furthermore, it can be observed that when comparing to experimental data the general features of this discharge profiles are retained. However, when observing the general features of the profile plots for all 10 JET discharges the brief summary can be discussed as follows. Firstly, the simulation results of T_i, T_e, and n_e are in agreement within one order of magnitude with experimental measurements. Secondly, the general trend of the profile such as the inclination is similar in some results and different in others. This can be due to the limited availability of some experimental parameters and incompleteness of the model. And lastly, n_e profiles are usually in better agreement with experimental data than the others. This is because in BALDUR, the boundary condition for density equation is empirically determined from line average density (n_l) according to equation (10). On the contrary, the pedestal temperature (T_{ped}) is theoretically calculated according to equation (14) so the prediction accuracy should be less than that of empirical approach. This also can

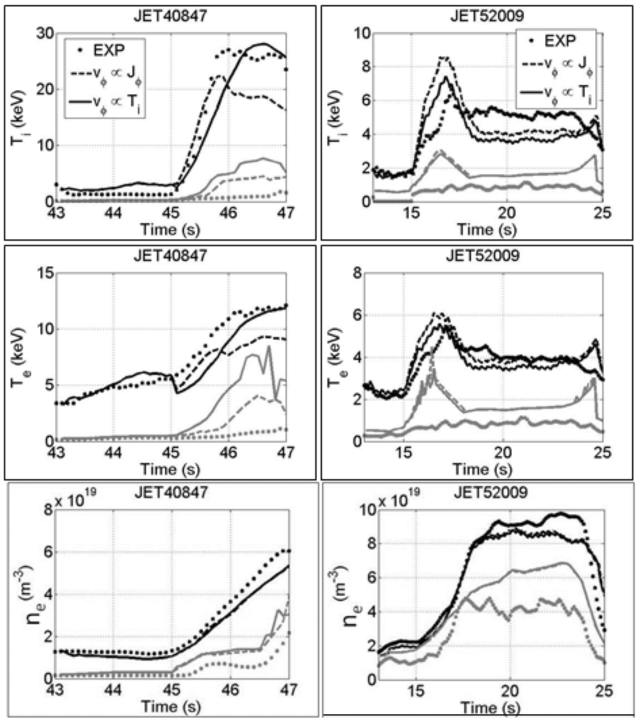

Figure 4. JET 40847 (left) and 52009 (right) time-evolution profiles of ion temperature T_i (top), electron temperature T_e (middle), and electron density n_e (bottom): experimental data (dots) simulation results using current density J_ϕ dependent (dashed) and ion temperature dependent (solid) models at the center (dark) and edge (gray) of the plasma.

be seen in Figure 4, in which the temperatures for both ion and electron at the edge are predicted much higher than that of the experiment, while the densities are predicted roughly closer to the experimental values.

Quantitatively, the three physical quantities profiles are compared with experimental data using the following normalized RMS comparison:

$$\mathrm{RMS}(\%) = \sqrt{\frac{1}{N}\sum_{i=1}^{N}\left(\frac{x_{\exp_i} - x_{\mathrm{mod}_i}}{x_{\exp_0}}\right)^2} \times 100, \qquad (18)$$

where x represents interested physical quantities (T_e, T_i, and n_e) and x_0 represents experimental data at the centre of the plasma. Note that in these comparisons, data of all grid positions in the plasma are included and of the entire duration that the discharge remains in H-mode. These results are shown as bar plots in Figure 5. For T_i comparison, the maximum of 41.48% is found in discharge 53532 of current density dependent model and the minimum of 18.14% is found in discharge 53521 of ion temperature dependent model. The averages of all discharges are 28.13±7.71% standard deviation for the current density dependent model, and 25.47±7.10% standard deviation for the ion temperature dependent model. For T_e comparison, the maximum of 63.74% is found in discharge 53532 of current density dependent model and the minimum of 14.88% is found in discharge 40847 of the same model. The averages of all discharges are 31.78±14.51% standard deviation for the current density dependent model, and 30.19±13.64% standard deviation for the ion temperature dependent model. For n_e comparison, the maximum of 21.54% is found in discharge 52009 of ion temperature dependent model and the minimum of 9.66% is found in discharge 46664 of the same model. The averages of all discharges are 15.00±3.23% standard deviation for the current density dependent model, and 15.15±3.50% standard deviation for the ion temperature dependent model. On average, it cannot be concluded which model is better because they are within the standard deviation of each other. This conclusion is different from the toroidal velocity prediction where it can be clearly seen that the ion temperature dependent model predicts better. This shows that the simulations profiles are not so much sensitive to the toroidal velocity profile. Nevertheless, if one observes the performance of each discharge simulation individually, one can find that on some discharge like 46664 the difference is significant in which the empirical model performs better.

4.1.3 ITB Formation

One physical phenomenon that is important to explore in this work is the ability of this suite of code to simulate ITB formation. This v_ϕ model is developed to explain the velocity in toroidal direction which is used to calculate the shearing rate ω_{ExB}, the cause of ITB formation. ITB formation can be found in either ion or electron channel, or both channels at the same time depending on heating method. Since the main heating in JET is either NBI (neutral beam injection) or ICRF (ion cyclotron resonance frequency) or both, ITB formations are found mainly in ion temperature profile so the work on ITB identification will be in T_i profile plots. ITB is defined as a local region of steep temperature gradient. So, the gradient will be used in order to identify ITB location and time of its occurrence.

Figure 6 illustrates the contour plot of ion temperature gradient spatiotemporal profiles with darker area representing relative higher temperature gradient area, showing examples for JET discharges 46664 and 53532. Only ion temperature profiles are shown here because BALDUR simulations yield similar qualitative behaviour for ion and electron profiles. Moreover, there is no ITB formation in the particle channels from these experiments. In this sense, the figure can be used to trace the location and the time evolution of the ITB. The top panels are experimental data, the

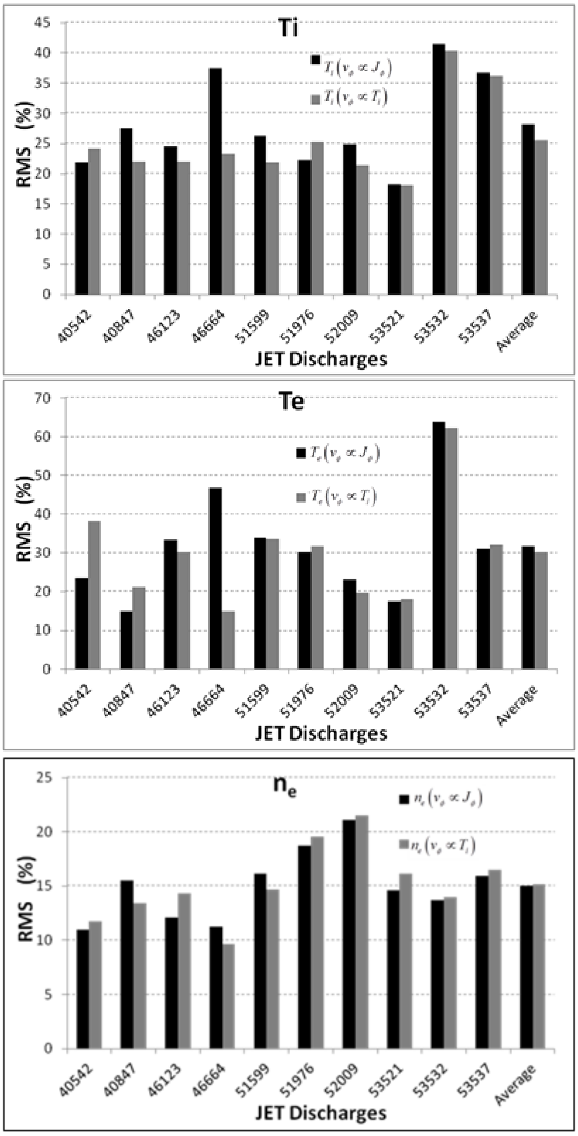

Figure 5. RMS deviations of 10 JET discharges and their averages for ion temperature T_i, electron temperature T_e, and electron density n_e simulation results using current density J_ϕ dependent (dark) and ion temperature T_i dependent (gray) models.

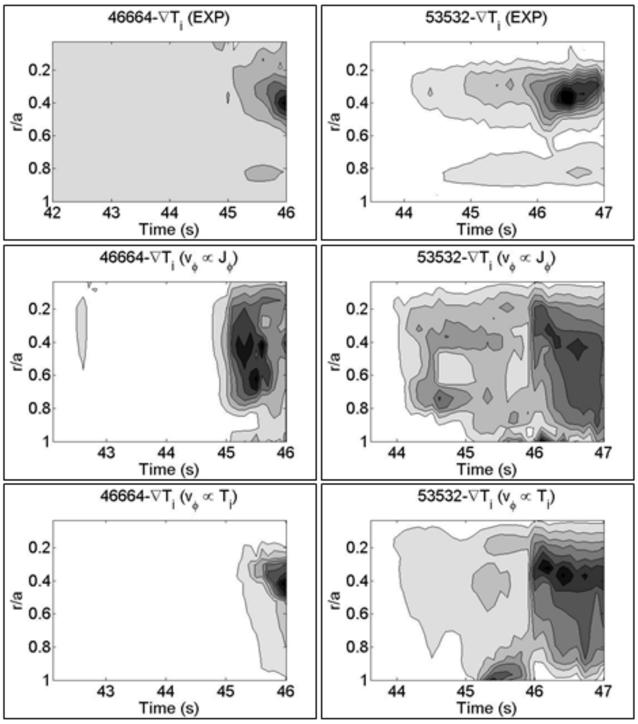

Figure 6. Contour plots of ion temperature gradient ∇T_i profile of JET discharge 40542: experimental results (top) and simulation results using current density J_ϕ dependent (middle) and ion temperature T_i dependent (bottom) models.

middle panels are the simulation results from current density dependent model and the bottom panels are simulation results from ion temperature dependent model. In discharge 46664, ITB forms around the time of 45.5 seconds near the position $r/a = 0.4$. It appears that the empirical model predicts almost the exact time of formation with a location slightly shifted toward $r/a = 0.5$. On the contrary, the current density dependent model predicts a wider ITB from $r/a = 0.4$ to 0.8 with formation time as early as 45 seconds. In discharge 53532, ITB forms around the time of 46 seconds near the position $r/a = 0.4$. Similar to the previous discharge, the empirical model predicts ITB formation better for both its time and location. Current density dependent model predicts softer ITB but for wider region. As a summary, from this qualitative observation, the empirical model predicts formation of ITB better. These results are as expected because, as mentioned earlier, the empirical model was derived from these discharges so they should fit the experimental results better. However, it is more interesting to see how it projects into a larger machine like ITER.

4.2 ITER predictions

ITER is an international collaboration with the main goal of demonstrating scientific and engineering feasibility of nuclear fusion machine (Aymar *et al.*, 2002). In this work, a standard type I ELMy *H*-mode ITER is chosen. Its design parameters are shown in Table 2, where RF represents radio frequency heating scheme and NBI represents neutral beam injection heating scheme, and the details of the operation scenario can be found in Onjun *et al.* (2009).

4.2.1 ITER performance and ITB effect

Figure 7 illustrates simulations of ITER for ion temperature (T_i), electron temperature (T_e), deuterium density (n_D), tritium density (n_T), beryllium density (n_{Be}), and helium density (n_{He}) as a function of normalized minor radius *r/a* at the time of 2,700 seconds. Note that at this time, the plasma has reached quasi-steady state condition as observed from Figure 8 that the plasma becomes relatively steady after 200 seconds. In both figures, the solid line is for simulation using

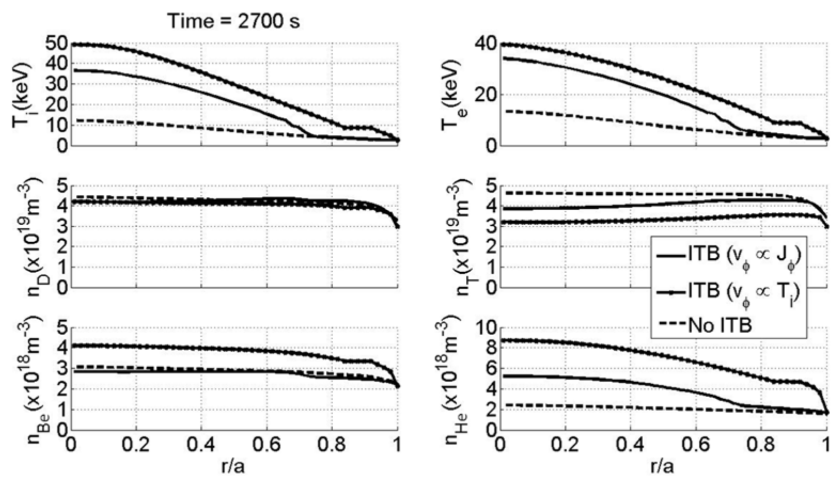

Figure 7. Comparison of ITER performance (for ion temperature T_i, electron temperature T_e, deuterium density n_D, tritium density n_T, beryllium density n_{Be}, and helium density n_{He}) between simulations with ITB (both current density and ion temperature dependent models) and without ITB effect during steady state (t = 2700 s).

Table 2. Engineering design parameters for ITER.

Parameters	unit	Values
R	m	6.2
a	m	2.0
I_p	MA	15.0
B_ϕ	T	5.3
κ	-	1.7
δ	-	0.33
RF	MW	7.0
NBI	MW	33.0
n_l	m^{-3}	$1.0\mathrm{x}10^{20}$

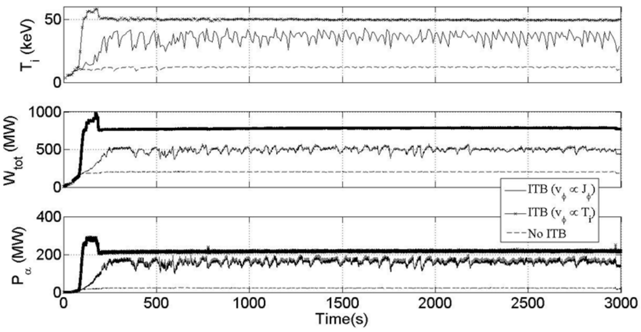

Figure 8. Time-evolution plots of central ion temperature T_i (top), total fusion power output W_{tot} (middle), and alpha power $P_á$ (bottom) for simulations with ITB (both current density J_ϕ and ion temperature T_i dependent models) and without ITB effect during steady state (t = 2700 s).

current density dependent model, the solid line with bullet is for simulation using ion temperature dependent model, and the dashed line is for simulation without ITB. It can be seen in Figure 7 that both temperatures are high near the center and lower toward the edge (from 3 to 10 times reduction), while the densities of all species remain roughly the same throughout the plasma (around 2 times or less reduction) except helium density in ITB simulation which accumulates more toward the plasma center (at most 4 times reduction).

The temperature profiles indicate the existence of ITB formations which is shown by significant improvements of plasma temperature over those results without ITB. It can be seen that when ITB effects are included in the simulation, the central temperature for both ion and electron increase significantly, from 12 keV to 38 keV (current density dependent) and 49 keV (ion temperature dependent), and from 13 keV to 33 keV (current density dependent) and 39 keV (ion temperature dependent), respectively. Yet, the temperatures near the edge of plasma remain approximately the same. This implies that ITB formations indeed result in better plasma confinement for the plasma temperature, hence energy. This also shows that the empirical model predicts higher values for ITER by around 20% for ion and 15% for electron temperatures at plasma center.

The bottom right panel shows that helium impurity accumulates more in the plasma core for simulations with ITB included, also in the ion temperature dependent model more than in the current density dependent model. This agrees with the trend in central temperatures which results in higher fusion reaction. Additionally, it means that ITB formations also prevent transport of impurity species especially helium. Beryllium is an impurity from the first wall outside of the plasma, the concentration is slightly higher in plasma with the ion temperature dependent model run as expected because there are more beryllium trapped in the core. However, the current density dependent model appears to show similar beryllium accumulation to that of simulation without ITB. The situation is similar for helium species, except that the concentration in the run with ITB effect is much higher than the run without ITB effect. As stated earlier, transport barriers improve plasma energy confinement and power production, which mean the fusion reaction rate is enhanced as well. This is confirmed by Figure 8 in the bottom panel which shows the time-evolution profile of alpha power. During quasi-steady state, the alpha powers of ITB simulations are almost 10 times higher than that without ITB formation. These alpha particles are not neutral so they are trapped by the magnetic field inside the tokamak. The energy is used to reheat the plasma, transferred back to deuterium and tritium by way of collision. More alpha power means more alpha particles produced from fusion reaction so higher helium density is observed. This result is further confirmed by deuterium and tritium density plots in Figure 7. Since both species are starting particles of the fusion reaction, a higher reaction rate implies more fuel burnt and hence less density accumulated for both. As observed from the figure, ITB simulation shows lower tritium and slightly lower deuterium concentrations.

In summary, to see what is happening at the center of the plasma, the central ion temperature is plotted as functions of time (Figure 8) along with total fusion power output and alpha power of the plasma. As expected, they are higher in simulations with ITB formation. Initially, during current ramp-up phase the profiles increase steeply and reach maximum around 100 seconds before dropping down because of the high radiation power to reach quasi-steady state. During this latter state, the average values of central ion temperature are 36 and 49 keV, of the total power outputs of the plasma are 492 and 800 MW, and of the alpha powers are 159 and 218 MW for the current density dependent and ion temperature dependent models, respectively. Note that the ion temperature dependent model provides more steady plasma profiles while the results from current density dependent model are much rather fluctuated.

It is interesting to observe how ITB forms in ITER using the two toroidal rotation models. Figure 9 illustrates the contour plots of the ion temperature gradient profiles. The top panel shows that the current density dependent model predicts ITB to be locally located around r/a = 0.7 with some slight fluctuations. Once formed, its location is

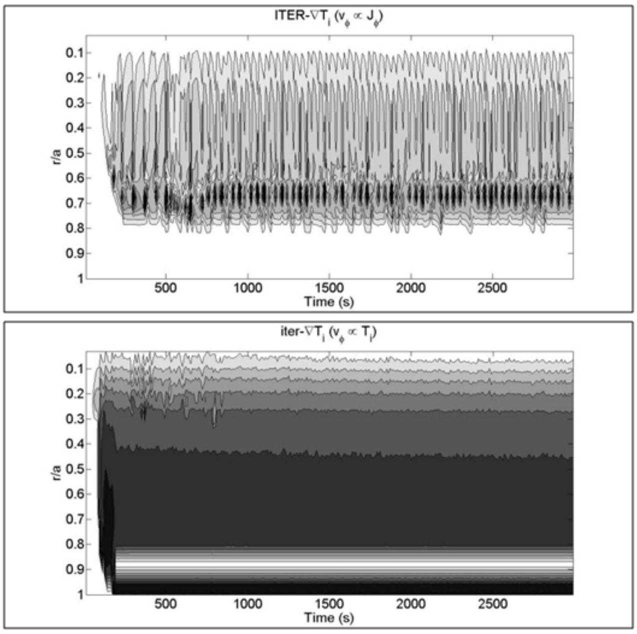

Figure 9. Contour plots of ion temperature gradient ∇T_i profile of ITER simulations: simulation results using current density J_ϕ dependent (top) and ion temperature T_i dependent (bottom) models.

moving in and out around the position. It also appears to collapse and reform. However, the period of collapsing and reformation is not regular or deterministic; future investigation is required. On the contrary, the ITB region from empirical model appears to be much wider, from *r/a* = 0.5 to 0.8. This agrees with what could be observed in the top panels of Figure 7, in which the strong gradient from the current density dependent model can be easily identified at *r/a* = 0.7 but not so for the ion temperature dependent model because it covers a wider region. This also explains why the empirical model yields higher temperature profiles, as it has a wider region of ITB, the transport reduction is much stronger. The toroidal velocity and the flow shear profiles are shown in Figure 10. It can be observed that in the simulation using current density dependent model, there exists a spike feature representing strong shear of the profiles at the vicinity of the ITB location. So there is a correlation between the location of the strong shear of toroidal velocity and ω_{ExB} flow shear profiles with that of temperature gradient or ITB. Moreover, the plasma appears to be rotated much faster, toroidally, in the simulation using empirical model. This will be physically quite challenging in ITER since NBI, as implied by the empirical model, should not be able to rotate the bigger machine that fast.

4.2.2 Test for plasma ignition

Plasma reaches an ignition condition if the auxiliary heating (NBI plus RF heating) is shut down but the plasma is still able to self-sustain. It is very important to study this issue for ITER because self-heating leads to possibility of long duration operation for fusion reactor. In this study, BALDUR code is used to simulate the similar ITER performance as before but the auxiliary heating is turned off after 2000 s, at which point the plasma has reached a quasi-steady state. After that, the plasma is solely heated by ohmic heating and alpha heating.

It is found in Figure 11 that ion temperatures, total powers and alpha powers drop as soon as the external heating is shutdown. Nevertheless, the plasma adjusts to a new quasi-steady state shortly after with lower temperatures and powers. In simulation without ITB effects included, the operation continues for about 400 seconds longer before reaching disruption because alpha heating diminishes as soon as auxiliary heating is off and then ohmic heating carries on the operation until the operation stops. Note that ohmic heating is small compared to other heating modes. With ITB effects included, the plasma achieves a new quasi-steady state at central ion temperatures of around 30 and 40 keV, total powers of 400 and 650 MW and alpha powers of 110 and 180 MW, for current density dependent and ion temperature dependent models, respectively. Note that ITB formations are still maintained even after auxiliary heating is turned off as shown in Figure 12 but the values of temperatures are slightly lower.

5. Conclusions

Self-consistent simulations of ITER with the presence of both ITB and ETB are carried out using the BALDUR code.

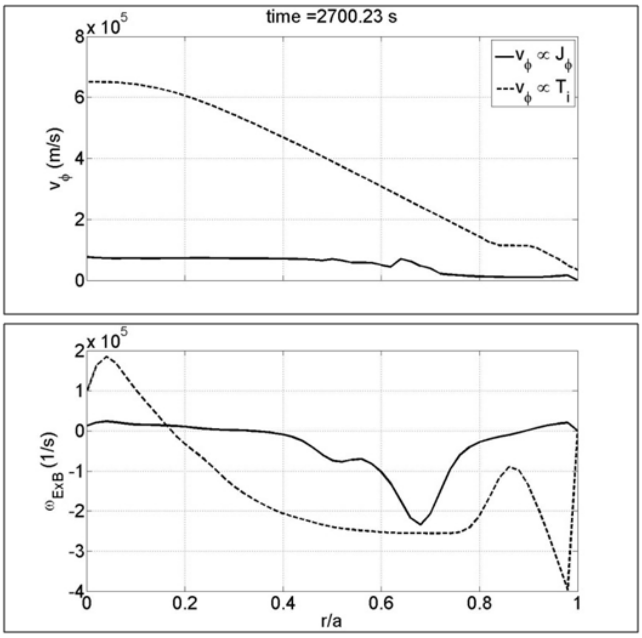

Figure 10. Toroidal velocityand flow shear ω_{ExB} profiles of simulations results for current density J_ϕ dependent (solid) and ion temperature T_i dependent (dashed) models during steady state (t = 2700 s).

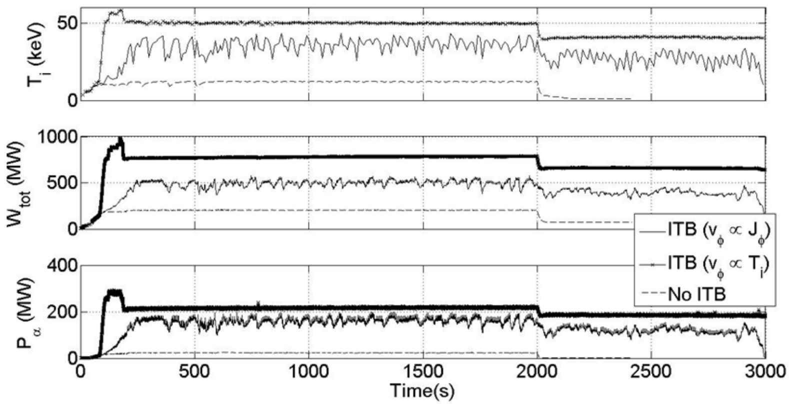

Figure 11. Time-evolution plots of central ion temperature T_i (top), total fusion power output W_{tot} (middle), and alpha power P_α (bottom) for simulations with ITB (both current density J_ϕ and ion temperature T_i dependent models) and without ITB effect during steady state (t = 2700 s), auxiliary heating is turned off after 2000 s.

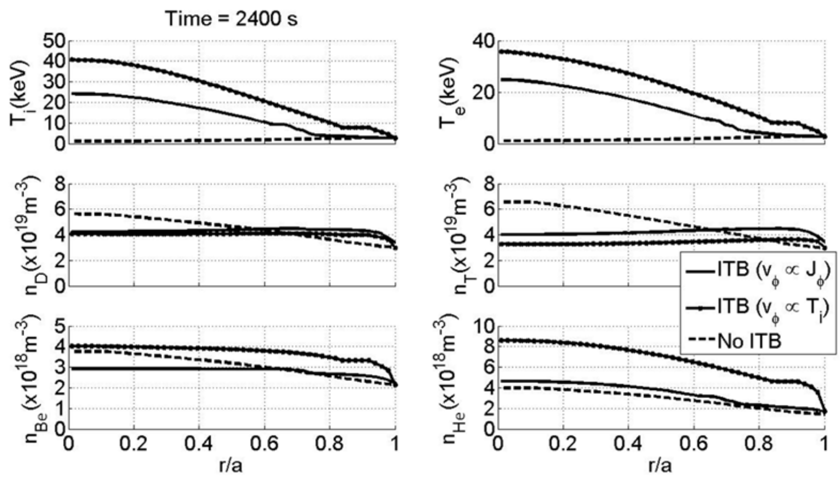

Figure 12. ITER performance simulations (for ion temperature T_i, electron temperature T_e, deuterium density n_D, tritium density n_T, beryllium density n_{Be}, and helium density n_{He}) with ITB (both current density and ion temperature dependent models) and without ITB effect at time after auxiliary heating is turned off (t = 2400 s).

The combination of Mixed B/gB transport model together with pedestal model based on magnetic and flow shear stabilization pedestal width scaling and an infinite-n ballooning pressure gradient model, and with two toroidal velocity models based on ion temperature and current density of the plasma, is used to simulate the time-evolution profiles of plasma temperature, density, and current for JET optimized shear discharges and ITER standard type I ELMy *H*-mode operation. It is found that the simulations with the ion temperature dependent toroidal velocity model yield better agreement with JET experimental data. For ITER prediction, the ion temperature dependent model yields more optimistic predictions but the current density dependent model predicts a rather narrow region of ITB. The presence of ITB is very crucial for ITER because it results in greater plasma energy confinement over standard run without ITB effects. The presence of ITB causes both ion and electron temperatures to be higher, especially at the center. However, it only slightly affects the densities of deuterium, tritium, and beryllium. Helium concentration is higher in ITB simulation because of a higher fusion reaction rate. Therefore, this is a critical issue for ITER. In addition, when the auxiliary heating is turned off, it is found that the core temperature, total power and alpha power are decreased slightly. Nevertheless, significant fusion energy still remains. The ignition condition cannot be achieved without the formations of ITB.

Acknowledgments

This work was supported by the Commission on Higher Education (CHE) and the Thailand Research Fund (TRF) under contract No.RSA5580041, the National Research University Project of Thailand Office of Higher Education Commission, and Low Carbon scholarship from Bangchak Petroleum PCL. B Chatthong thanks the Royal Thai Scholarship for monthly support.

References

Artaud, J. F., Basiuk, V., Imbeaux, F., Schneider, M., Garcia, J., Giruzzi, G., Huynh, P., Aniel, T., Albajar, F., Ané, J. M., Bécoulet, A., Bourdelle, C., Casati, A., Colas, L., Decker, J., Dumont, R., Eriksson, L. G., Garbet, X., Guirlet, R., Hertout, P., Hoang, G. T., Houlberg, W., Huysmans, G., Joffrin, E., Kim, S. H., Köchl, F., Lister, J., Litaudon, X., Maget, P., Masset, R., Pégourié, B., Peysson, Y., Thomas, P., Tsitrone, E., and Turco, F. 2010. The CRONOS suite of codes for integrated tokamak modelling. Nuclear Fusion. 50, 043001.

Aymar, R., Barabaschi, P., and Shimomura, Y. 2002. The ITER design. Plasma Physics and Controlled Fusion. 44, 519.

Bateman, G., Onjun, T., and Kritz, A. H. 2003. Integrated predictive modelling simulations of burning plasma experiment designs. Plasma Physics and Controlled Fusion. 45, 1939.

Boucher, D., Connor, J. W., Houlberg, W. A., Turner, M. F., Bracco, G., Chudnovskiy, A., Cordey, J. G., Greenwald, M. J., Hoang, G. T., Hogeweij, G. M. D., Kaye, S. M., Kinsey, J. E., Mikkelsen, D. R., Ongena, J., Schissel, D. R., Shirai, H., Stober, J., Stubberfield, P. M., Waltz, R. E., Weiland, J., and The ITER 1D Modelling Working Group. 2000. The International Multi-Tokamak Profile Database. Nuclear Fusion. 40, 1955.

Budny, R. V., Andre, R., Bateman, G., Halpern, F., Kessel, C. E., Kritz, A., and McCune, D. 2008. Predictions of H-mode performance in ITER. Nuclear Fusion. 48, 075005.

Burrell, K. H. 1997. Effects of E x B velocity shear and magnetic shear on turbulence and transport in magnetic confinement devices. Physics of Plasmas. 4, 1499-1518.

Callen, J. D., Cole, A. J., and Hegna, C. C. 2009. Toroidal rotation in tokamak plasmas. Nuclear Fusion. 49, 085021.

Cenacchi, G., and Taroni, A. 1988. JETTO: a free boundary plasma transport code. ENEA Report RT/TIB. 88, 5.

Chatthong, B., Onjun, T., and Singhsomroje, W. 2010. Model for toroidal velocity in H-mode plasmas in the presence of internal transport barriers. Nuclear Fusion. 50, 064009.

Chatthong, B., and Onjun, T. 2011. Self-Consistent Simulation of Standard *H*-Mode ITER with the Presence of an Internal Transport Barrier. Thammasat International Journal of Science and Technology. 16, 42-53.

Chatthong, B., and Onjun, T. 2013. Simulations of ITER in the presence of ITB using the NTV intrinsic toroidal rotation model. Nuclear Fusion. 53, 013007.

Connor, J. W. 1998. A review of models for ELMs. Plasma Physics and Controlled Fusion. 40, 191.

Connor, J. W., Fukuda, T., Garbet, X., Gormezano, C., Mukhovatov, V., Wakatani, M., the ITB Database Group, and the ITPA Topical Group on Transport and Internal Barrier Physics. 2004. A review of internal transport barrier physics for steady-state operation of tokamaks. Nuclear Fusion. 44, R1.

Diamond, P. H., Itoh, S.-I., Itoh, K., and Hahm, T. S. 2005. Zonal flows in plasma—a review. Plasma Physics and Controlled Fusion. 47, R35.

Erba, M., Parail, V., Springmann, E., and Taroni, A. 1995. Extension of a Bohm model for L-mode electron heat transport to ion heat transport and to the ohmic regime. Plasma Physics and Controlled Fusion. 37, 1249.

Eriksson, A., Nordman, H., Strand, P., Weiland, J., Tala, T., Asp, E., Corrigan, G., Giroud, C., Greef, M. d., Jenkins, I., Knoops, H. C. M., Mantica, P., Rantamäki, K. M., Vries, P. C. d., Zastrow, K.-D., and JET EFDA Contributors. 2007. Predictive simulations of toroidal momentum transport at JET. Plasma Physics and Controlled Fusion. 49, 1931.

Halpern, F. D., Kritz, A. H., Bateman, G., Pankin, A. Y., Budny, R. V., and McCune, D. C. 2008. Predictive simulations of ITER including neutral beam driven toroidal rotation. Physics of Plasmas. 15, 062505.

Hannum, D., Bateman, G., Kinsey, J., Kritz, A. H., Onjun, T., and Pankin, A. 2001. Comparison of high-mode predictive simulations using Mixed Bohm/gyro-Bohm and Multi-Mode (MMM95) transport models. Physics of Plasmas. 8, 964-974.

Houlberg, W. A., Shaing, K. C., Hirshman, S. P., and Zarnstorff, M. C. 1997. Bootstrap current and neoclassical transport in tokamaks of arbitrary collisionality and aspect ratio. Physics of Plasmas. 4, 3230-3242.

Kinsey, J. E., Staebler, G. M., and Waltz, R. E. 2002. Simulations of internal transport barrier formation in tokamak discharges using the GLF23 transport model. Physics of Plasmas. 9, 1676-1691.

Klaywitthaphat, P., and Onjun, T. 2012. Simulations of plasma behavior during pellet injection in ITER. Plasma Physics Reports. 38, 496-502.

Leekhaphan, P., and Onjun, T. 2011. Pellet Injection into H_mode ITER Plasma with the Presence of Internal Transport Barriers. Plasma Physics Reports. 37, 321-327.

Onjun, T., Bateman, G., Kritz, A. H., and Hammett, G. 2002. Models for the pedestal temperature at the edge of H-mode tokamak plasmas. Physics of Plasmas. 9, 5018-5030.

Onjun, T., Kritz, A. H., Bateman, G., and Parail, V. 2005. Magnetohydrodynamic-calibrated edge-localized mode model in simulations of International Thermonuclear Experimental Reactor. Physics of Plasmas. 12, 082513.

Onjun, T., and Pianroj, Y. 2009. Simulations of ITER with combined effects of internal and edge transport barriers. Nuclear Fusion. 49, 075003.

Parail, V. V., Baranov, Y. F., Challis, C. D., Cottrell, G. A., Fischer, B., Gormezano, C., Huysmans, G. T. A., Litaudon, X., Sips, A. C. C., Söldner, F. X., Springmann, E. M., Taroni, A., and Ward, D. J. 1999. Predictive modelling of JET optimized shear discharges. Nuclear Fusion. 39, 429.

Parail, V. V. 2002. Energy and particle transport in plasmas with transport barriers. Plasma Physics and Controlled Fusion. 44, A63.

Pereverzev, G., and Yushmanov, P. N. 2002. ASTRA Automated System for Transport Analysis in a Tokamak. Max-Planck Institut fur Plasmaphysik. IPP 5/98.

Pianroj, Y., Chuchinda, C., Leekhaphan, P., and Onjun, T. 2010. Behaviors of Impurity in ITER Plasma with Standard Type I ELMy H-mode and Steady State Scenarios. Plasma Physics Reports. 36, 827.

Pianroj, Y., Techakunchaiyanunt, J., and Onjun, T. 2012. Model for Pedestal Transport Based on Suppression of Anomalous Transport Using ùExB Flow Shear and Magnetic Shear. Journal of the Physical Society of Japan. 81, 044502.

Roach, C. M., Walters, M., Budny, R. V., Imbeaux, F., Fredian, T. W., Greenwald, M., Stillerman, J. A., Alexander, D. A., Carlsson, J., Cary, J. R., Ryter, F., Stober, J., Gohil, P., Greenfield, C., Murakami, M., Bracco, G., Esposito, B., Romanelli, M., Parail, V., Stubberfield, P., Voitsekhovitch, I., Brickley, C., Field, A. R., Sakamoto, Y., Fujita, T., Fukuda, T., Hayashi, N., Hogeweij, G. M. D., Chudnovskiy, A., Kinerva, N. A., Kessel, C. E., Aniel, T., Hoang, G. T., Ongena, J., Doyle, E. J., Houlberg, W. A., Polevoi, A. R., ITPA Confinement Database Modelling Topical Group, and ITPA Transport Physics Topical Group. 2008. The 2008 Public Release of the International Multi-tokamak Confinement Profile Database. Nuclear Fusion. 48, 125001.

Rogister, A. L., Rice, J. E., Nicolai, A., Ince-Cushman, A., Gangadhara, S., and Alcator C-Mod Group. 2002. Theoretical interpretation of the toroidal rotation velocity observed in Alcator C-Mod Ohmic H-mode discharges. Nuclear Fusion. 42, 1144.

Rozhansky, V., Kaveeva, E., Voskoboynikov, S., Coster, D., Bonnin, X., and Schneider, R. 2002. Modelling of electric fields in tokamak edge plasma and L-H transition. Nuclear Fusion. 42, 1110.

Singer, C. E., Post, D. E., Mikkelsen, D. R., Redi, M. H., McKenney, A., Silverman, A., Seidl, F. G. P., Rutherford, P. H., Hawryluk, R. J., Langer, W. D., Foote, L., Heifetz, D. B., Houlberg, W. A., Hughes, M. H., Jensen, R. V., Lister, G., and Ogden, J. 1988. Baldur: A one-dimensional plasma transport code. Computer Physics Communications. 49, 275-398.

Stacey, W. M. 2004. A neoclassical model for toroidal rotation and the radial electric field in the edge pedestal. Physics of Plasmas. 11, 3096-3099.

Sugihara, M., Igitkhanov, Y., Janeschitz, G., Hubbard, A. E., Kamada, Y., Lingertat, J., Osborne, T. H., and Suttrop, W. 2000. A model for H mode pedestal width scaling using the International Pedestal Database. Nuclear Fusion. 40, 1743.

Tala, T., Laborde, L., Mazon, D., Moreau, D., Corrigan, G., Crisanti, F., Garbet, X., Heading, D., Joffrin, E., Litaudon, X., Parail, V., Salmi, A., and contributors to the EFDA-JET workprogramme. 2005. Predictive transport simulations of real-time profile control in JET advanced tokamak plasmas. Nuclear Fusion. 45, 1027.

Tala, T., Imbeaux, F., Parail, V. V., Bourdelle, C., Corrigan, G., Garbet, X., Heading, D. J., Litaudon, X., Strand, P. I., Weiland, J., and JET-EFDA contributors. 2006. Fully predictive time-dependent transport simulations of ITB plasmas in JET, JT-60U and DIII-D. Nuclear Fusion. 46, 548.

Tala, T., Crombé, K., Vries, P. C. d., Ferreira, J., Mantica, P., Peeters, A. G., Andrew, Y., Budny, R., Corrigan, G., Eriksson, A., Garbet, X., Giroud, C., Hua, M.-D., Nordman, H., Naulin, V., Nave, M. F. F., Parail, V., Rantamäki, K., Scott, B. D., Strand, P., Tardini, G., Thyagaraja, A., Weiland, J., Zastrow, K.-D., and JET-EFDA Contributors. 2007. Toroidal and poloidal momentum transport studies in tokamaks. Plasma Physics and Controlled Fusion. 49, B291.

Tala, T. J. J., Heikkinen, J. A., Parail, V. V., Baranov, Y. F., and Karttunen, S. J. 2001. ITB formation in terms of $\omega E\times B$ flow shear and magnetic shear s on JET. Plasma Physics and Controlled Fusion. 43, 507.

Tala, T. J. J., Parail, V. V., Becoulet, A., Corrigan, G., Heading, D. J., Mantsinen, M. J., Strand, P. I., and contributors to the EFDA-JET Workprogramme. 2002. Comparison of theory-based and semi-empirical transport modelling in JET plasmas with ITBs. Plasma Physics and Controlled Fusion. 44, A495.

Taroni, A., Erba, M., Springmann, E., and Tibone, F. 1994. Global and local energy confinement properties of simple transport coefficients of the Bohm type. Plasma Physics and Controlled Fusion. 36, 1629.

Wagner, F., Becker, G., Behringer, K., Campbell, D., Eberhagen, A., Engelhardt, W., Fussmann, G., Gehre, O., Gernhardt, J., Gierke, G. v., Haas, G., Huang, M., Karger, F., Keilhacker, M., Klüber, O., Kornherr, M., Lackner, K., Lisitano, G., Lister, G. G., Mayer, H. M., Meisel, D., Müller, E. R., Murmann, H., Niedermeyer, H., Poschenrieder, W., Rapp, H., and Röhr, H. 1982. Regime of Improved Confinement and High Beta in Neutral-Beam-Heated Divertor Discharges of the ASDEX Tokamak. Physical Review Letters. 49, 1408.

Wesson, J., and Campbell, D. J. 2004. Tokamaks, Clarendon Press ; Oxford University Press, New York, U.S.A.

Wisitsorasak, A., and Onjun, T. 2011. Impacts of Pellets Injected from the Low Field Side on Plasma in ITER. Plasma Physics Reports. 37, 1-18.

Zhu, P., Bateman, G., Kritz, A. H., and Horton, W. 2000. Predictive transport simulations of internal transport barriers using the Multi-Mode model. Physics of Plasmas. 7, 2898-2908.